Electron-electron interactions and doping dependence of the two-phonon Raman intensity in graphene

D. M. Basko,[1,*] S. Piscanec,[2] and A. C. Ferrari[2]

[1]*Laboratoire de Physique et Modélisation des Milieux Condensés, Université Joseph Fourier and CNRS, 38042 Grenoble, France*

[2]*Department of Engineering, Cambridge University, 9 JJ Thomson Avenue, Cambridge CB3 OFA, United Kingdom*

(Received 8 June 2009; revised manuscript received 15 September 2009; published 16 October 2009)

Raman spectroscopy is a fast and nondestructive means to characterize graphene samples. In particular, the Raman spectra are strongly affected by doping. While the resulting change in position and width of the *G* peak can be explained by the nonadiabatic Kohn anomaly at Γ, the significant doping dependence of the 2*D* peak intensity has not been understood yet. Here we show that this is due to a combination of electron-phonon and electron-electron scattering. Under full resonance, the photogenerated electron-hole pairs can scatter not just with phonons but also with doping-induced electrons or holes, and this changes the intensity. We explain the doping dependence and show how it can be used to determine the corresponding electron-phonon coupling. This is higher than predicted by density-functional theory, as a consequence of renormalization by Coulomb interactions.

DOI: 10.1103/PhysRevB.80.165413 PACS number(s): 78.30.−j, 73.50.Bk

I. INTRODUCTION

Graphene is the latest carbon allotrope discovered and it is now at the center of a significant research effort.[1–6] Near-ballistic transport at room temperature and high mobility[5–10] make it a potential material for nanoelectronics,[11–14] especially for high-frequency applications.[15] Furthermore, its transparency and mechanical properties are ideal for micromechanical and nanomechanical systems, thin-film transistors, transparent and conductive composites and electrodes, and photonics.[16–20]

Graphene layers can be readily identified in terms of number and orientation by inelastic and elastic light scattering such as Raman[21] and Rayleigh spectroscopies.[22,23] Raman spectroscopy also allows monitoring of doping, defects, strain, disorder, chemical modifications, and edges.[21,24–38] Indeed, Raman spectroscopy is a fast and nondestructive characterization method for carbons.[39] They show common features in the 800–2000 cm^{-1} region: the *G* and *D* peaks, around 1580 and 1350 cm^{-1}, respectively. The *G* peak corresponds to the E_{2g} phonon at the Brillouin-zone center (**Γ** point). The *D* peak is due to the breathing modes of six-atom rings and requires a defect for its activation.[38,40,41] It comes from TO phonons around the **K** point of the Brillouin zone,[38,41] is active by double resonance (DR),[40] and is strongly dispersive with excitation energy due to a Kohn Anomaly at **K**.[27] The activation process for the *D* peak is intervalley and is shown schematically in Fig. 1(d): (i) a laser-induced excitation of an electron/hole pair; (ii) electron-phonon scattering with an exchanged momentum $\mathbf{q}\sim\mathbf{K}$; (iii) defect scattering; (iv) electron-hole recombination. DR can also happen as intravalley process, i.e., connecting two points belonging to the same cone around **K** (or **K**′), as shown in Fig. 1(b). This gives the so-called *D*′ peak, which is at about 1620 cm^{-1} in defected graphite, when measured at 514 nm excitation.

The 2*D* peak is the second order of the *D* peak. This is a single peak in single-layer graphene (SLG) whereas it splits into four in bilayer graphene (BLG), reflecting the evolution of the band structure.[21] The 2*D*′ peak is the second order of the *D*′ peak. Since both 2*D* and 2*D*′ originate from a process where momentum conservation is satisfied by two phonons with opposite wave vectors (**q** and **−q**), they do not require the presence of defects for their activation and are thus always present. Indeed, high-quality graphene shows the *G*, 2*D*, and 2*D*′ peaks but not *D* and *D*′.[21] Also, under the

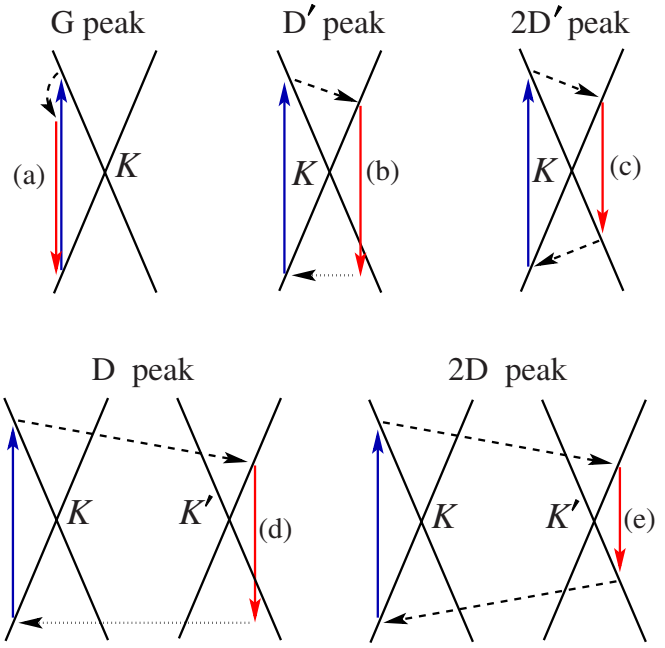

FIG. 1. (Color online) Role of the electron dispersion (Dirac cones, $\epsilon=\pm v_F|\mathbf{p}|$, shown by solid black lines) in Raman scattering: (a) intravalley one-phonon *G* peak, (b) defect-assisted intravalley one-phonon *D*′ peak, (c) intravalley two-phonon 2*D*′ peak, (d) defect-assisted intervalley one-phonon *D* peak, and (e) intervalley two-phonon 2*D* peak. Vertical solid arrows represent interband transitions accompanied by photon absorption (upward arrows) or emission (downward arrows) (the photon wave vector is neglected). Dashed arrows represent phonon emission. Horizontal dotted arrows represent defect scattering.

 ©2009 The American Physical Society

assumption of electron-hole symmetry, the two-phonon peaks are fully resonant.[42,43] This means that energy and momentum conservation are satisfied in all elementary steps of the Raman process, as shown schematically in Figs. 1(c) and 1(e). Then, all intermediate electronic states are real. As a consequence, two-phonon Raman spectroscopy is sensitive to the dynamics of the photoexcited electron-hole pair, in particular, to the scattering processes it can undergo. This is of crucial importance for the present work.

Doping in graphene is commonly observed in as-deposited samples, due to the presence of charges at the surface or interface.[24,44] It can also be induced by applying a voltage on an external gate electrode.[26,32,33,36] Substitutional doping, either bulk or edge, is also possible,[45,46] however, thus far, these samples are far from ideal, and the effects of doping and structural disorder overlap in their Raman spectrum.[45] In the present work we will thus focus on the variation in the Raman spectra observed in samples where the Fermi level moves as a result of charged impurities or applied voltages, or both, as reported in Refs. 24, 26, 32, 33, and 36. The G peak position, Pos(G), increases and its full width at half maximum, FWHM(G), decreases for both electron and hole doping. The G peak stiffening is due to the nonadiabatic removal of the Kohn anomaly at $\mathbf{\Gamma}$.[26,47] The FWHM(G) sharpening is due to Pauli blocking of phonon decay into electron-hole pairs, when the electron-hole gap is higher than the phonon energy,[26,48] and saturates for a Fermi shift bigger than half phonon energy.[26,36,48] A similar behavior is observed for the LO-G^- peak in metallic nanotubes,[49] for the same reasons. In the case of BLG, the different band structure renormalizes the phonon response to doping differently from SLG.[33,50,51] Also in this case the Raman G peak stiffens and sharpens for both electron and hole doping, as a result of the nonadiabatic Kohn anomaly at $\mathbf{\Gamma}$.[33] However, since BLG has two conduction and valence subbands, with splitting dependent on the interlayer coupling, this changes the slope in the variation in Pos(G) with doping, allowing a direct measurement of the interlayer coupling strength.[33,51]

Another significant result is that in SLG the ratio of the heights of the 2D and G peaks, $I(2D)/I(G)$, and their areas, $A(2D)/A(G)$, is maximum for zero doping,[21,52] and decreases for increasing doping. On the other hand, this shows little dependence on doping for BLG.[32,33] Figure 2 plots the combined data for SLG and BLG from Refs. 21, 32, 33, 52, and 53. Note that Refs. 32 and 33 reported height ratios, while here, as discussed later, we analyze the area ratio $A(2D)/A(G)$, which encompasses both trends of $I(2D)/I(G)$ and FWHM(2D)/FWHM(G).

Due to residual disorder, the energy of the Dirac point can fluctuate across the sample on a scale smaller than the laser spot, which leads to spatial inhomogeneity of the doping level.[24,44] We attribute the difference in the behavior of the two SLG curves in Fig. 2 to a different degree of residual charge inhomogeneity in the polymeric electrolyte experiments of Refs. 32 and 33. On the other hand, the use of this electrolyte enabled probing a very large doping range because the nanometer-thick Debye layer gives a much higher gate capacitance compared to the usual 300 nm SiO_2 back gate.[26,32,33] Note as well that $A(2D)/A(G)$ for the most intrinsic samples measured to date is about 12–17,[21,52,53] much higher than the zero gating values in Refs. 32 and 33, as shown in Fig. 2. This points again to sources of disorder in the gated samples of Refs. 32 and 33, while the absence of a significant D peak excludes large amounts of structural defects. Finally, we stress that all data for varying E_F in Fig. 2 are measured on samples on Si covered by the same SiO_2 thickness, thus the relative change in peaks' intensities with doping is not related to extrinsic interference effects.[22,54]

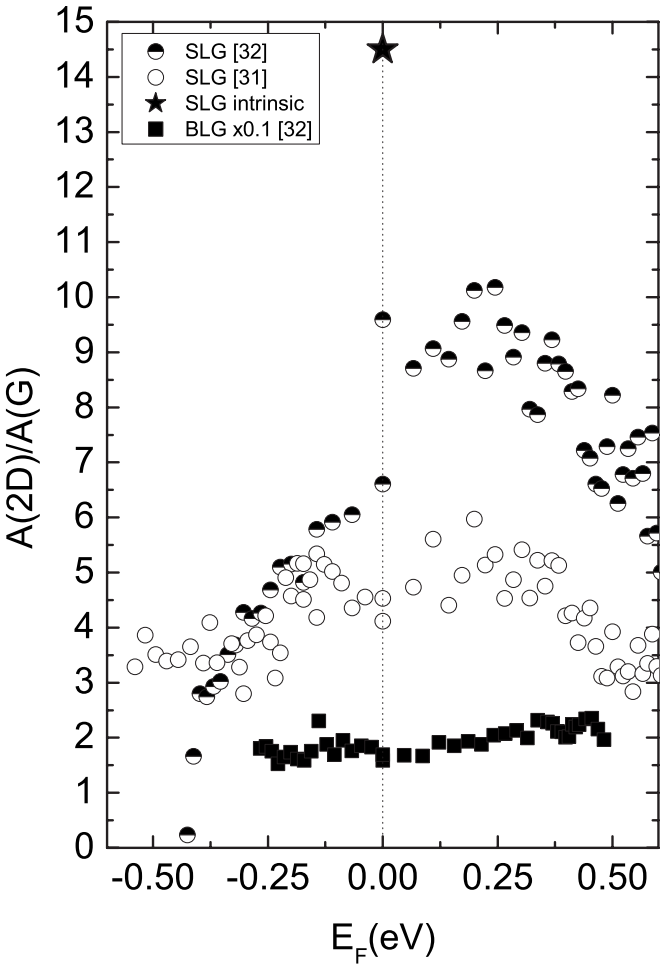

FIG. 2. Experimental $A(2D)/A(G)$, measured for 514.5 nm excitation, as a function of E_F for SLG (Refs. 21, 32, 33, and 52) and BLG (Ref. 33). The BLG data (solid squares) are divided by ten, to make comparison easier. Note that the doping-dependent SLG data are a combination of two experiments on two different samples, from Ref. 33 (half-filled circles) and Ref. 32 (open circles), and a data-point representative of intrinsic graphene from Refs. 21, 52, and 53 (solid star).

Here, we show that the dependence on doping of the 2D peak intensity results from its sensitivity to the scattering of the photoexcited electron and hole. Assuming the dominant sources of scattering to be phonon emission and electron-electron collisions, we note that while the former is not sensitive to doping, the latter is. Then, the 2D doping dependence can be used to estimate the corresponding electron-phonon coupling (EPC).

II. DOPING DEPENDENCE OF TWO-PHONON RAMAN INTENSITY

A. Theoretical dependence

Raman scattering[55] is an electron-mediated process where electromagnetic radiation exchanges vibrational quanta (phonons) with a crystal. A complete description requires the detailed knowledge of (i) electronic structure, (ii) phonon dispersions, and (iii) mutual interactions between electrons and phonons (i.e., electron-electron, electron-phonon, and phonon-phonon scattering).

The Raman spectrum of graphene consists of a set of distinct peaks. Each characterized by its position width, height, and area. The frequency-integrated area under each peak represents the probability of the whole process. It is more robust with respect to various perturbations of the phonon states than width and height. Indeed, for an ideal case of dispersionless undamped phonons with frequency ω_{ph} the shape of the n-phonon peak is a Dirac δ distribution $\propto\delta(\omega-n\omega_{\mathrm{ph}})$, with zero width, infinite height but well-defined area. If the phonons decay (e.g, into other phonons, due to anharmonicity, or into electron-hole pairs, due to electron-phonon coupling), the δ peak broadens into a Lorentzian, but the area is preserved, as the total number of phonon states cannot be changed by such perturbations. If phonons have a weak dispersion, states with different momenta contribute at slightly different frequencies. This may result in an overall shift and a nontrivial peak shape but frequency integration across the peak means counting all phonon states, as in the dispersionless case. Thus, the peak area is preserved, as long as the Raman matrix element itself is not changed significantly by the perturbation. The latter holds when the perturbation (phonon broadening or dispersion) is smaller than the typical energy scale determining the matrix element. Converting this into a time scale using the uncertainty principle we obtain that, if the Raman process is faster than the phonon decay, the total number of photons emitted within a given peak (i.e., integrated over frequency across the peak), is not affected by phonon decay, although their spectral distribution can be. Even if the graphene phonons giving rise to the D and D' peaks are dispersive due to the Kohn anomalies at **K** and **Γ**,[27] their relative change with respect to the average phonon energy is at most a few percent, thus we are in the weakly dispersive case discussed above. The phonon decay in graphene is in the picosecond time scale, while the Raman process is faster, in the femtosecond time scale.[26,56,57] Then, we will analyze the area ratio, $A(2D)/A(G)$, which encompasses both variations in height ratio, $I(2D)/I(G)$, and width $\mathrm{FWHM}(2D)/\mathrm{FWHM}(G)$.

We first consider the G peak. For the one-phonon process, allowed by momentum conservation, which gives rise to the G peak, the picture is entirely different from the two-phonon case. As shown in Fig. 1(a), the process responsible for the G peak is determined by virtual electrons and holes with energy $\sim E_L/2$, where E_L is the laser excitation energy (for a typical Raman measurement $E_L/2\sim 1$ eV). If the Fermi energy, E_F, stays below $E_L/2$, as in Refs. 32 and 33, these electronic states are not strongly affected. Only the final phonon state is influenced by doping, which manifests itself in a change in $\mathrm{Pos}(G)$ and $\mathrm{FWHM}(G)$.[26,32,33,36] However, the area of the peak is determined by the total spectral weight of the phonon state, which is preserved. Thus, we do not expect any significant dependence of $A(G)$ on doping, as long as the doping is not too strong, $|E_F|\ll 1$ eV. We can then take the measured doping dependence of $A(2D)/A(G)$ as representative of the $A(2D)$ trend. Note that $A(G)$ can change as a function of other external parameters such as the Raman excitation energy.[21,38,58–60] However, for fixed excitation, such as in the experiments discussed here, the above argument holds.

In Ref. 43 the following expressions for the $2D$ and $2D'$ areas were obtained:

$$A(2D)=\frac{8}{3}\left(\frac{e^2}{c}\right)^2\frac{v_F^2}{c^2}\left(\frac{\gamma_K}{\gamma}\right)^2, \tag{1a}$$

$$A(2D')=\frac{4}{3}\left(\frac{e^2}{c}\right)^2\frac{v_F^2}{c^2}\left(\frac{\gamma_\Gamma}{\gamma}\right)^2, \tag{1b}$$

where e is the electron charge, c is the speed of light, $e^2/c\approx 1/137$ is the fine-structure constant, and v_F is the electron velocity (its experimental value is $v_F\approx 10^6$ m/s≈ 6.6 eV Å (Refs. 61–63). 2γ is the scattering rate of the photoexcited electron and hole. Note that we define γ as the imaginary part of the energy, so it determines the decay of the amplitude, while the decay of the probability is determined by 2γ. This includes all sources of inelastic scattering. Assuming the two main mechanisms for electron scattering to be the emission of phonons and electron-electron collisions, we write

$$\gamma=\gamma_{\text{e-ph}}+\gamma_{\mathrm{ee}},\quad \gamma_{\text{e-ph}}=\gamma_\Gamma+\gamma_K. \tag{2}$$

Here we include the phonons near **Γ** and **K**, responsible for D and D'. The corresponding emission rates, $2\gamma_\Gamma$ and $2\gamma_K$, enter the numerators in Eqs. (1a) and (1b).

Two points regarding Eqs. (1a) and (1b) should be emphasized. First, the scattering rates depend on the electron energy, ϵ, which is defined by half the laser energy, $\epsilon\approx E_L/2$ [see Eq. (9) in the next section]. Second, if impurity scattering is significant compared to other scattering mechanisms, the corresponding elastic-scattering rate cannot be simply included in γ and Eqs. (1a) and (1b). The whole Raman intensity calculation should be done differently. Equations (1a) and (1b) thus neglect impurity scattering. For short-range impurities this assumption is justified by the absence of a large D peak in the spectra of Refs. 32 and 33. Long-range disorder is efficiently screened (even though the vanishing density of states at the Dirac point requires the screening to be nonlinear[64–67]); it is precisely this screening that gives rise to the inhomogeneous concentration of electrons/holes and spatial fluctuations of the Dirac-point energy.

In principle, there are no reasons for a strong dependence of $\gamma_{\text{e-ph}}$ on carrier density. However, γ_{ee} does exhibit such a dependence. Indeed, in undoped graphene at low temperatures, the photoexcited electron finds itself in a state with some momentum, **p**, measured from the Dirac point, in the empty conduction band. To scatter into a state with a different momentum **p**′, it has to give away some energy and momentum to another electron in the full valence band. This

second electron would have to be promoted to the conduction band (as there are no available empty states in the valence band) into a state with momentum $\mathbf{p}_e$, leaving a hole in the valence band with momentum $\mathbf{p}_h$. Momentum and energy conservation require

$$\mathbf{p} = \mathbf{p}' + \mathbf{p}_e + \mathbf{p}_h, \tag{3a}$$

$$\epsilon(\mathbf{p}) = \epsilon(\mathbf{p}') + \epsilon(\mathbf{p}_e) + \epsilon(\mathbf{p}_h), \tag{3b}$$

where $\epsilon(\mathbf{p})$ is the quasiparticle dispersion, assumed the same for electrons and holes. For Dirac particles $\epsilon(\mathbf{p})=v_F|\mathbf{p}|$, so the only possibility to satisfy both conservation laws is to have all four momenta parallel. If the spectrum is convex, $d^2\epsilon(p)/dp^2>0$, the two equations can be satisfied by a set of momenta with nonzero measure, i.e., the phase space is finite. If it is concave, $d^2\epsilon(p)/dp^2<0$, they are incompatible. In SLG the spectrum is Dirac to a first approximation, resulting in an uncertainty.[68] This can be resolved by taking into account corrections from electron-electron interactions, which make the spectrum concave[69,70] and the interband process forbidden.

As new carriers are added to the system, intraband electron-electron collisions become allowed. The momentum and energy conservation become

$$\mathbf{p} + \mathbf{p}_e = \mathbf{p}' + \mathbf{p}_e', \tag{4a}$$

$$\epsilon(\mathbf{p}) + \epsilon(\mathbf{p}_e) = \epsilon(\mathbf{p}') + \epsilon(\mathbf{p}_e'), \tag{4b}$$

which can be satisfied for any quasiparticle dispersion. These collisions give a contribution to γ_{ee} which increases with carrier concentration. As a consequence, the total γ in Eq. (1a) increases, leading to an overall decrease in $A(2D)$, consistent with the experimental trend in Fig. 2.

The above arguments essentially use the nonconvexity of the electronic spectrum in the conduction band, and thus apply to SLG only. In BLG the spectrum is parabolic near the Dirac point, so that $d^2\epsilon/dp^2>0$, and the phase-space restrictions are absent. Thus, electron-electron collisions are allowed even at zero doping and the collision rate has a much weaker dependence on E_F, which, in first approximation, can be neglected. Thus, $A(2D)$ is expected to have a weak dependence on E_F, as seen in Fig. 2, where the experimental $A(2D)/A(G)$ for BLG shows a negligible variation with doping.[33]

To quantify the doping effects on the SLG $A(2D)$, we first calculate the electron-electron scattering rate, $2\gamma_{ee}$, in the random-phase approximation, analogously to Refs. 71 and 72. γ_{ee} is given by the imaginary part of the on-shell electronic self-energy, Im $\Sigma_{ee}(p,\epsilon)$ for $\epsilon \to v_F p - 0^+$, with ϵ and $\mathbf{p}$ counted from the Dirac point.[68] Here we consider the limiting case, when the energy of the photoexcited electron ($\epsilon=E_L/2$) far exceeds E_F. The carrier concentration is $n=E_F^2/(\pi v_F^2)$. In this case, the collisions are dominated by small momentum transfers, $|\mathbf{p}-\mathbf{p}'|\sim|E_F|/v_F$, so γ_{ee} does not depend on ϵ and is proportional to $|E_F|$, the proportionality coefficient depending only on the dimensionless Coulomb coupling constant $r_s=e^2/(\varepsilon v_F)$ (ε being the dielectric constant),

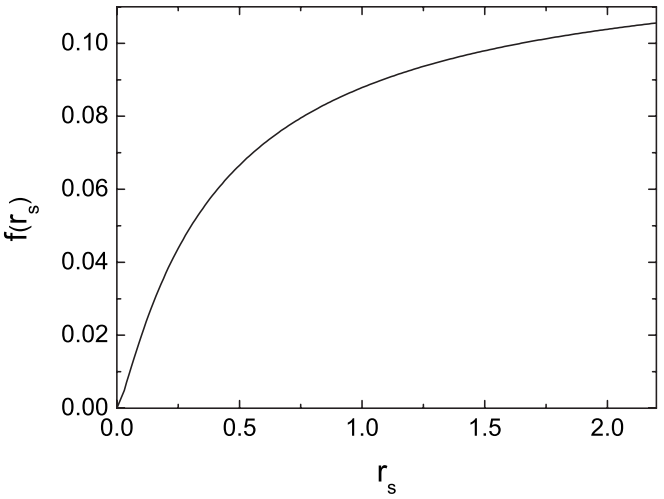

FIG. 3. Numerical values of the function $f(r_s)$, appearing in Eq. (5).

$$\gamma_{ee} = |E_F| f\left(\frac{e^2}{\varepsilon v_F}\right) + O(E_F^2/\epsilon). \tag{5}$$

The explicit form of the function f is given in the Appendix. Figure 3 plots its numerical values for $r_s<2.2$, corresponding to $\varepsilon>1$.

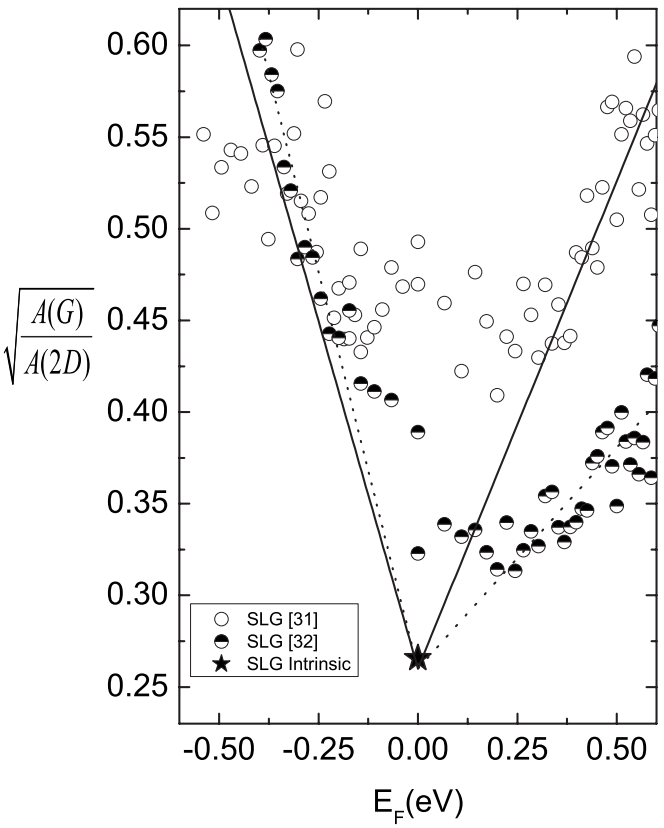

FIG. 4. Fit of the experimental dependence $\sqrt{A(G)/A(2D)}$ from Ref. 32 (open circles), Ref. 33 (half-filled circles), and the data for intrinsic graphene (Refs. 21, 52, and 53) (star) using Eq. (8) (dashed and solid lines, respectively).

Thus, we expect $A(2D)$ to change with E_F as

$$A(2D) = \frac{C}{[\gamma_{\text{e-ph}} + |E_F| f(e^2/\varepsilon v_F)]^2} \tag{6}$$

with C a constant. Note that a variation in the dielectric constant ε will affect $A(2D)$. Given the negligible dependence of $A(G)$ on doping, Eq. (6) can be rewritten as

$$\sqrt{\frac{A(G)}{A(2D)}} = C'[\gamma_{\text{e-ph}} + |E_F| f(e^2/\varepsilon v_F)], \tag{7}$$

where C' is another constant.

B. Fit to experiments

Figure 4 plots $\sqrt{A(G)/A(2D)}$ as a function of E_F. This dependence, according to Eq. (7), should correspond to two symmetric straight lines joining at $E_F=0$. As noted in Sec. I, close to $E_F=0$ the data from the two polymer electrolyte gating experiments do not converge to the same value. However, for both a linear rise of $\sqrt{A(G)/A(2D)}$ is seen at higher energies. Also, while the data represented by open circles in Fig. 4 are almost symmetric, a significant asymmetry is seen for electron doping in the set represented by the half-filled circles, but the two sets are in good agreement for hole doping.

$A(2D)/A(G)$ for intrinsic samples measured at 514.5 nm excitation, the same as in Refs. 32 and 33, is in the range 12–17,[21,52] represented by the star in Fig. 2 at 14.5, corresponding to $\sqrt{A(G)/A(2D)}=0.26$ at $E_F=0$. This is in good agreement with the ratio measured for carbon whiskers.[53] These show a $2D$ peak very similar to graphene, being composed of misoriented graphene layers.[53,73] However, their Raman spectra are much less susceptible to charged impurities or surface doping, being bulk materials.[53] We also need to consider the dielectric constant of the polymer electrolyte used in the experiment of Ref. 32, $\varepsilon=5$, giving $f(e^2/\varepsilon v_F) \approx 0.06$. Thus, we fit the data with a one-parameter expression

$$\sqrt{\frac{A(G)}{A(2D)}} = \frac{0.26}{\gamma_{\text{e-ph}}}(\gamma_{\text{e-ph}} + 0.06|\epsilon_F|). \tag{8}$$

We fit separately each branch of the two data sets, as shown by solid and dotted lines in Fig. 4. As a result, we obtain $\gamma_{\text{e-ph}}=18, 21, 29, 65$ meV, with an average $\gamma_{\text{e-ph}}=33$ meV.[74]

III. RAMAN INTENSITIES AND ELECTRON-PHONON COUPLING

A. Theoretical background and electron-phonon coupling definitions

Even though graphite and other sp^2-hybridized materials have been investigated for more than 60 years,[41,75] all the fundamental physical properties needed for the interpretation of the Raman spectra have undergone an intense debate, which seems to be just beginning to converge. Interestingly, several features of both phonon dispersions and band structure of graphene are determined by the EPC. For example, in the Kohn anomalies around $\mathbf{\Gamma}$ or $\mathbf{K}$ (Ref. 27) the correction to the phonon frequencies due to EPC results in a linear slope of the optical phonon branches as the wave vector approaches $\mathbf{\Gamma}$ or $\mathbf{K}$. The EPC and phonon-dispersions calculations of Ref. 27 have been confirmed at the $\mathbf{\Gamma}$ point by inelastic x-ray scattering[76] and by the measurement of FWHM(G) in graphite, graphene, and nanotubes,[21,26,48,77] once anharmonic effects are taken into account.[21,26,56] For the $\mathbf{K}$ point, the precise slope of the anomaly is still debated.[37,78,79] Another EPC effect is the kink in the electron dispersion, about 200 meV below E_F, seen by angle-resolved photoemission spectroscopy (ARPES).[63,80] This is attributed to a correction to the electron energy due to EPC,[63,80,81] although alternative explanations also exist.[82] Thus, a correct EPC determination is a fundamental step for an accurate description of the physical properties of graphene and nanotubes, these being rolled up graphene sheets.

To link the $2D$ intensity to the EPC we first consider the rate of phonon emission by the photoexcited electron/hole, $2\gamma_{\text{e-ph}}$. This is obtained from the imaginary part of the electron self-energy, $\gamma_{\text{e-ph}}=\text{Im}\,\Sigma_{\text{e-ph}}(\epsilon)$. For $E_L/2 > E_F+\omega_\Gamma$, as in the case of the Raman measurements at 2.41 eV excitation of Refs. 32 and 33, we have[43]

$$\gamma_K = \frac{\lambda_K}{4}\left(\frac{E_L}{2} - \omega_K\right), \quad \gamma_\Gamma = \frac{\lambda_\Gamma}{4}\left(\frac{E_L}{2} - \omega_\Gamma\right). \tag{9}$$

Then, from Eq. (2)

$$\gamma_{\text{e-ph}} = \frac{\lambda_K}{4}\left(\frac{E_L}{2} - \omega_K\right) + \frac{\lambda_\Gamma}{4}\left(\frac{E_L}{2} - \omega_\Gamma\right). \tag{10}$$

The dimensionless coupling constants $\lambda_\Gamma, \lambda_K$ correspond to phonons close to $\mathbf{\Gamma}$ and $\mathbf{K}$, respectively, and determine their rate of emission. We define them as

$$\lambda_{\Gamma,K} = \frac{F_{\Gamma,K}^2 A_{\text{u.c.}}}{2M\omega_{\Gamma,K} v_F^2}. \tag{11}$$

Here $\omega_K=1210\ \text{cm}^{-1}=0.150$ eV (Ref. 79) and $\omega_\Gamma=1580\ \text{cm}^{-1}=0.196$ eV,[21] $M \approx 2.00\times10^{-23}$ g$=2.88\times10^3$ (eV Å^2)$^{-1}$ is the mass of the carbon atom and $A_{\text{u.c.}} \approx 5.24$ Å^2 is the unit-cell area. F_Γ and F_K have the dimensionality of a force and are the proportionality coefficients between the change in effective Hamiltonian and the lattice displacement along the corresponding phonon mode. Strictly speaking, the relevant phonon states are not exactly at $\mathbf{\Gamma}$ and $\mathbf{K}$, as shown in Fig. 1. However, the corresponding deviation, $q \sim E_L/v_F$, is small compared to the $\mathbf{K}-\mathbf{K}'$ distance and is neglected. All observables depend on the dimensionless EPCs, λ_Γ and λ_K.

Equation (11) follows the notation of Ref. 43. Since different EPC definitions are used in the literature, it is quite useful to give here matching rules for all of them, which will be necessary when comparing the EPC values obtained here with previous (and future) reports. The EPCs can be conveniently matched by either relating them to the nearest-neighbor tight-binding model, where they are expressed in terms of a single parameter, $\partial t_0/\partial a$, the derivative of the nearest-neighbor electronic matrix element with respect to the interatomic distance, or by comparing expressions for various observables. For example, doping leads to a G peak

shift due to EPC. This is expressed in terms of E_F as[26,36,47,83]

$$\delta\omega_\Gamma = \frac{\lambda_\Gamma}{2\pi}\left(|E_F| + \frac{\omega_\Gamma}{4}\ln\frac{2E_F-\omega_\Gamma}{2E_F+\omega_\Gamma}\right). \tag{12}$$

The corrections to the phonon dispersions as function of wave vector $\mathbf{q}$, measured from $\mathbf{\Gamma}$ or $\mathbf{K}$, are[27,43,77]

$$\delta\omega_{\Gamma-\mathrm{LO}} = \frac{\lambda_\Gamma}{8}\sqrt{v_F^2q^2-\omega_\Gamma^2}, \tag{13a}$$

$$\delta\omega_{\Gamma-\mathrm{TO}} = -\frac{\lambda_\Gamma}{8}\frac{\omega_\Gamma^2}{\sqrt{v_F^2q^2-\omega_\Gamma^2}}, \tag{13b}$$

$$\delta\omega_K = \frac{\lambda_K}{4}\sqrt{v_F^2q^2-\omega_K^2}. \tag{13c}$$

Note that the E_{2g} mode splits into longitudinal ($\Gamma-$LO) and transverse ($\Gamma-$TO) at finite q. Note also that due to analytical properties of the logarithm and the square root, Eq. (12) at $|E_F|<\omega_\Gamma/2$ and Eqs. (13a)–(13c) at $v_Fq<\omega_{K,\Gamma}$ acquire imaginary parts, which correspond to the phonon decaying into a continuum of electron-hole pairs.[48] In this case 2 Im $\delta\omega$ gives the FWHM of the corresponding Lorentzian profile. At $v_Fq \gg \omega_{K,\Gamma}$ Eqs. (13a) and (13c) give the profile of the Kohn anomalies.

In Refs. 26, 27, 78, and 84 the EPCs are defined as the matrix elements of the Kohn-Sham potential, differentiated with respect to the phonon displacements. What enters the observables are their squares, averaged over the Fermi surface in the limit $E_F\to 0$. The matching rule is then

$$F_\Gamma^2 = 4\langle D_\mathbf{\Gamma}^2\rangle_F^{(\text{Refs. 26 and 78})} = 8M\omega_\Gamma\langle g_\mathbf{\Gamma}^2\rangle_F^{(\text{Refs. 27 and 84})}, \tag{14a}$$

$$F_K^2 = 2\langle D_\mathbf{K}^2\rangle_F^{(\text{Refs. 26 and 78})} = 4M\omega_K\langle g_\mathbf{K}^2\rangle_F^{(\text{Refs. 27 and 84})}. \tag{14b}$$

In Refs. 36 and 83 the dimensionless coupling constant λ is defined as the proportionality coefficient in Eq. (12). Thus,

$$\lambda^{(\text{Refs. 36 and 83})} = \frac{\lambda_\Gamma}{2\pi}. \tag{15}$$

Note that the expression linking EPC to FWHM(G) in Ref. 36 underestimates FWHM(G) by a factor 2, and should not be used.

The dimensionless EPCs reported in the ARPES analysis of Refs. 63, 80, 85, and 86 and in the scanning tunneling spectroscopy (STS) experiment of Ref. 87 were measured from the ratio of the electronic velocities below and above the kink in the electron dispersion. This ratio is determined by the derivative of the real part of the electronic self-energy Re $\Sigma_{\text{e-ph}}(\epsilon)$ due to the EPC. The latter can be calculated if one takes the Dirac spectrum for electrons and a constant dispersion for phonons. For $E_F>0$ one has[84]

$$\begin{aligned}\Sigma_{\text{e-ph}}(\epsilon) = &-\frac{\lambda_K}{4\pi}(\epsilon-\omega_K)\ln\frac{E_M}{|\epsilon-\omega_K-E_F|}\\ &-\frac{\lambda_K}{4\pi}(\epsilon+\omega_K)\ln\frac{E_M|\epsilon+\omega_K-E_F|}{(\epsilon+\omega_K)^2}\\ &-\frac{\lambda_\Gamma}{4\pi}(\epsilon-\omega_\Gamma)\ln\frac{E_M}{|\epsilon-\omega_\Gamma-E_F|}\\ &-\frac{\lambda_\Gamma}{4\pi}(\epsilon+\omega_\Gamma)\ln\frac{E_M|\epsilon+\omega_\Gamma-E_F|}{(\epsilon+\omega_\Gamma)^2}.\end{aligned} \tag{16}$$

Here E_M is the ultraviolet cutoff, on the order of the electronic bandwidth. We then get the matching rule

$$\begin{aligned}\lambda^{(\text{kink})} &= -\left.\frac{\partial\,\text{Re}\,\Sigma_{\text{e-ph}}}{\partial\epsilon}\right|_{\epsilon=E_F}\\ &= \frac{\lambda_K}{2\pi}\left(\frac{E_F-\omega_K}{\omega_K}+\ln\frac{E_M}{\omega_K+E_F}\right)\\ &\quad+\frac{\lambda_\Gamma}{2\pi}\left(\frac{E_F-\omega_\Gamma}{\omega_\Gamma}+\ln\frac{E_M}{\omega_\Gamma+E_F}\right).\end{aligned} \tag{17}$$

However, we note that λ_K is subject to Coulomb renormalizations.[88] This implies that λ_K depends on the electronic energy scale, such as the electron energy ε, the Fermi energy E_F, or the temperature T, whichever is larger, $\lambda_K=\lambda_K(\max\{|\epsilon|,|E_F|,T\})$. This dependence is shown in Fig. 6 of Ref. 88. In a Raman measurement this scale is given by the energy of the photoexcited electron, $\epsilon\approx E_L/2$, as long as $E_L/2>|E_F|$. Thus, in Eq. (10) $\lambda_K=\lambda_K(E_L/2)$. On the other hand, to estimate the EPC effects on the phonon dispersions in intrinsic graphene, the relevant electron energy is on the order of the phonon energy. Thus, in Eq. (13c) $\lambda_K\sim\lambda_K(\omega_K)$. From Fig. 6 of Ref. 88 we estimate that $\lambda_K(\omega_K)/\lambda_K(E_L/2)\approx 1.5$ for $\varepsilon=1$ and 1.2 for $\varepsilon=5$ (taking $E_L\approx 2$ eV to represent Raman measurements in the visible range).

The situation with Eq. (17) is more complicated since the cutoff E_M appears explicitly. The logarithmic term is determined by *all* energy scales from E_M down to $E_F+\omega_K$. Thus, the proper expression is

$$\begin{aligned}\lambda^{(\text{kink})} &= \frac{\lambda_K(E_F)}{2\pi}\frac{E_F-\omega_K}{\omega_K}+\int_{E_F+\omega_K}^{E_M}\frac{\lambda_K(\epsilon)}{2\pi}\frac{d\epsilon}{\epsilon}\\ &\quad+\frac{\lambda_\Gamma}{2\pi}\left(\frac{E_F-\omega_\Gamma}{\omega_\Gamma}+\ln\frac{E_M}{E_F+\omega_\Gamma}\right).\end{aligned} \tag{18}$$

B. Experimental electron-phonon coupling

From Eq. (12), our overall average $\gamma_{\text{e-ph}}=33$ meV, derived from a fit to all the data in Fig. 4, gives

$$\lambda_\Gamma+\lambda_K\approx 0.13. \tag{19}$$

We also note that the hole doping side of Fig. 4 shows two data sets very consistent with each other. We can thus get another estimate taken from the average $\gamma_{\text{e-ph}}\approx 20$ meV for just the hole doping side. This would give

$$\lambda_\Gamma + \lambda_K \approx 0.08. \tag{20}$$

Based on measurements[26,36] and density-functional theory (DFT) calculations,[27] the value of λ_Γ can be reliably taken ≈ 0.03. Indeed, DFT gives[27] $\langle g_\Gamma^2 \rangle_F = 0.0405$ eV^2 and $v_F = 5.5$ eV Å, corresponding, from Eqs. (11) and (14a) to $\lambda_\Gamma \approx 0.028$. Even though $\langle g_\Gamma^2 \rangle_F$ and v_F are subject to Coulomb renormalization, $\lambda_\Gamma = 4A_{\text{u.c.}} \langle g_\Gamma^2 \rangle_F / v_F^2$, which contains their ratio, is not.[88] The experimental λ_Γ extracted from FWHM(G) in graphene and graphite[21,48] according to Eq. (13a) and from the dependence of Pos(G) on Fermi energy according to Eq. (12), are $\lambda_\Gamma \approx 0.034$ (Ref. 36) and $\lambda_\Gamma \approx 0.027$.[26]

On the other hand, the value of λ_K is still debated.[78,84,88] The calculated DFT $\langle g_{\mathbf{K}}^2 \rangle_F = 0.0994$ eV^2, together with the DFT $v_F = 5.5$ eV·Å (both taken from Ref. 27) gives $\lambda_K = 0.034$. However, Ref. 88 suggested this should be enhanced by Coulomb renormalization by up to a factor 3, depending on the background dielectric constant. In order to compare with our fits, we need consider that the corrections to the phonon dispersion are determined by electronic states with energies lower than those contributing to the Raman signal. As discussed in Sec. III A, $\lambda_K(\omega_K)/\lambda_K(E_L/2) \approx 1.2$ for $\varepsilon = 5$. Our fit in Eq. (19) corresponds to $\lambda_K(E_L/2) \approx 0.1$ while Eq. (20) gives $\lambda_K(E_L/2) \approx 0.05$, resulting in $\lambda_K(\omega_K) \approx 0.12$ and $\lambda_K(\omega_K) \approx 0.06$, respectively. These are bigger than DFT by a factor of about 3.5 and 1.7, respectively.

A recent GW calculation gave $\langle D_{\mathbf{K}}^2 \rangle_F = 193$ eV^2/Å^2.[78] Combining this with the GW value $v_F = 6.6$ eV Å,[89] we get $\lambda_K(\omega_K) \approx 0.054$, a factor ~ 1.6 greater than DFT, in good agreement with our fitted average on the hole side.

Ref. 79 reported inelastic x-ray scattering measurements of the phonon dispersions near **K** more detailed than those originally done in Ref. 76, now giving a phonon slope at **K** of 73 meV Å. Using Eq. (13c) at $q \gg \omega_K / v_F$ and taking the experimental value $v_F = 6.6$ eV Å (Ref. 63) (the bare electron velocity, i.e., below the phonon kink), we obtain $\lambda_K(\omega_K) \approx 0.044$, a factor ~ 1.3 higher than DFT, again in good agreement with our fitted average on the hole side.

Another EPC estimate can be derived from the $2D$ and $2D'$ area ratio. Combining Eqs. (1a), (1b), (9), and (10) we get

$$\frac{A(2D)}{A(2D')} = 2\left(\frac{\lambda_K}{\lambda_\Gamma}\right)^2. \tag{21}$$

For intrinsic SLG and graphite whiskers, the experimental ratio $A(2D)/A(2D')$ is about 25–30,[21,52,53] which gives $\lambda_K(E_L/2) \approx 0.11$ and $\lambda_\Gamma + \lambda_K(E_L/2) \approx 0.13$. Since in this case $\varepsilon = 1$, we obtain $\lambda_K(\omega_K) \approx 0.16$, 4.5 times higher than DFT, in agreement with our upper estimate from Eq. (19).

We finally consider the EPC derived from ARPES and STS. For an estimate, we approximate the dependence $\lambda_K(\epsilon)$ as linear in $\ln \epsilon$. We take $\lambda_K(E_M) = (\omega_\Gamma/\omega_K)\lambda_\Gamma$, as given by DFT (assumed to be valid at high energies), and leave $\lambda_K(E_L/2 \approx 1$ eV) as the only free parameter determining this linear dependence,

$$\lambda_K(\epsilon) = \frac{\omega_\Gamma}{\omega_K}\lambda_\Gamma - \left[\frac{\omega_\Gamma}{\omega_K}\lambda_\Gamma - \lambda_K(E_L/2)\right]\frac{\ln(E_M/\epsilon)}{\ln[E_M/(E_L/2)]}. \tag{22}$$

Taking $E_F = 0.4$ eV,[63,80,86,87] $E_M = 10$ eV, and substituting Eq. (22) in Eq. (18), we get

$$\lambda^{(\text{kink})} \approx 0.7\lambda_\Gamma + 0.6\lambda_K(E_L/2). \tag{23}$$

Note that the dependence on the precise value of E_M is weak; setting $E_M = 5$ eV changes the first coefficient to 0.5 and the second (more important as it multiplies the larger coupling constant) varies only by 2%. The measurements in Refs. 63, 80, and 85–87gave $\lambda^{(\text{kink})} \approx 0.4, 0.3, 0.26, 0.2, 0.14$, respectively. The smallest of these values, $\lambda^{(\text{kink})} \approx 0.14$, from Eq. (23) corresponds to $\lambda_\Gamma + \lambda_K(E_L/2) \approx 0.23$ while the highest to $\lambda_\Gamma + \lambda_K(E_L/2) \approx 0.66$. Even the smallest is almost twice our upper bound fit of Eq. (19) and would imply an EPC renormalization of almost 1 order of magnitude. Resolution effects could play a role in this overestimation.[84]

Thus, our fits to the doping-dependent Raman area ratios point to a significant renormalization, by a factor 1.7–3.5, of the EPC for the TO mode close to **K**, responsible for the Raman D and $2D$ peaks. Our lower bound estimate is consistent with recent GW calculations and phonon measurements, but our upper bound is much lower than the smallest estimate derived by ARPES, pointing to a problem in the way ARPES-based works have thus far extracted EPC from their experimental data.

IV. CONCLUSIONS

We have shown that the $2D$ intensity dependence on doping can be explained considering the influence of electron-electron interactions on the total scattering rate of the photogenerated electrons (holes). We have given a simple formula linking $2D$ peak area to the Fermi-level shift. Fitting this to the available experimental data we got an estimate for the EPC value of the TO phonons close to **K**, responsible for the Raman D and $2D$ peaks. This is larger than that from DFT calculations, due to renormalization by Coulomb interactions. However, our fitted EPC is still significantly smaller than those reported in ARPES or STS experiments.

ACKNOWLEDGMENTS

We acknowledge A. Das, S. Berciaud, A. Bonetti, and P. H. Tan for useful discussions. A.C.F. acknowledges funding from the Royal Society and the European Research Council grant NANOPOTS.

APPENDIX: THE FUNCTION $f(r_s)$

The function $f(r_s)$, appearing in Eq. (5), can be represented as

$$f(r_s) = \frac{2}{\pi}\int_0^{\pi/2} d\varphi \times \left\{ \int_0^{2/(1+\cos\varphi)} \frac{dx\ x^2 \sin\varphi R_1}{[2(x/r_s+4)x\sin\varphi]^2 + R_1^2} + \int_{2/(1+\cos\varphi)}^{2/(1-\cos\varphi)} \frac{dx\ x^2 \sin\varphi R_2}{[2(x/r_s+4)x\sin\varphi - R_3]^2 + R_2^2(x,\varphi)} \right\}, \tag{A1}$$

where R_1, R_2, and R_3 are given by

$$R_1(x,\varphi) = a_+ b_+ - a_- b_- - x^2 \ln\frac{a_+ + b_+}{a_- + b_-}, \tag{A2a}$$

$$R_2(x,\varphi) = a_+ b_+ - x^2 \ln\frac{a_+ + b_+}{x}, \tag{A2b}$$

$$R_3(x,\varphi) = a_- \sqrt{x^2 - a_-^2} - x^2 \arccos\frac{a_-}{x}, \tag{A2c}$$

$$a_\pm = 2 \pm x\cos\varphi, \quad b_\pm = \sqrt{a_\pm^2 - x^2}. \tag{A2d}$$

Figure 3 plots $f(r_s)$, calculated numerically.

*denis.basko@grenoble.cnrs.fr

[1] K. S. Novoselov, A. K. Geim, S. V. Morozov, D. Jiang, Y. Zhang, S. V. Dubonos, I. V. Grigorieva, and A. A. Firsov, Science **306**, 666 (2004).

[2] A. K. Geim and K. S. Novoselov, Nature Mater. **6**, 183 (2007).

[3] A. H. Castro Neto, F. Guinea, N. M. R. Peres, K. S. Novoselov, and A. K. Geim, Rev. Mod. Phys. **81**, 109 (2009).

[4] J. C. Charlier, P. C. Eklund, J. Zhu, and A. C. Ferrari, in *Carbon nanotubes*, edited by A. Jorio, G. Dresselhaus, and M. S. Dresselhaus (Springer, Berlin, 2008).

[5] K. S. Novoselov, A. K. Geim, S. V. Morozov, D. Jiang, M. I. Katsnelson, I. V. Grigorieva, S. V. Dubonos, and A. A. Firsov, Nature (London) **438**, 197 (2005).

[6] Y. Zhang, Y. W. Tan, H. L. Stormer, and P. Kim, Nature (London) **438**, 201 (2005).

[7] K. S. Novoselov, Z. Jiang, Y. Zhang, S. V. Morozov, H. L. Stormer, U. Zeitler, J. C. Maan, G. S. Boebinger, P. Kim, and A. K. Geim, Science **315**, 1379 (2007).

[8] S. V. Morozov, K. S. Novoselov, M. I. Katsnelson, F. Schedin, D. C. Elias, J. A. Jaszczak, and A. K. Geim, Phys. Rev. Lett. **100**, 016602 (2008).

[9] X. Du, I. Skachko, A. Barker, and E. Y. Andrei, Nat. Nanotechnol. **3**, 491 (2008).

[10] K. I. Bolotin, K. J. Sikes, J. Hone, H. L. Stormer, and P. Kim, Phys. Rev. Lett. **101**, 096802 (2008); K. I. Bolotin, K. J. Sikes, Z. Jiang, G. Fundenberg, J. Hone, P. Kim, and H. L. Stormer, Solid State Commun. **146**, 351 (2008).

[11] M. Y. Han, B. Özyilmaz, Y. Zhang, and P. Kim, Phys. Rev. Lett. **98**, 206805 (2007).

[12] Z. Chen, Y. M. Lin, M. Rooks, and P. Avouris, Physica E (Amsterdam) **40**, 228 (2007).

[13] Y. Zhang, J. P. Small, W. V. Pontius, and P. Kim, Appl. Phys. Lett. **86**, 073104 (2005).

[14] M. C. Lemme, T. J. Echtermeyer, M. Baus, and H. Kurz, IEEE Electron Device Lett. **28**, 282 (2007).

[15] Y. M. Lin, K. A. Jenkins, A. Valdes-Garcia, J. P. Small, D. B. Farmer, and P. Avouris, Nano Lett. **9**, 422 (2009).

[16] J. S. Bunch, A. M. van der Zande, S. S. Verbridge, I. W. Frank, D. M. Tanenbaum, J. M. Parpia, H. G. Craighead, and P. L. McEuen, Science **315**, 490 (2007).

[17] P. Blake, P. D. Brimicombe, R. R. Nair, T. J. Booth, D. Jiang, F. Schedin, L. A. Ponomarenko, S. V. Morozov, H. F. Gleeson, E. W. Hill, A. K. Geim, and K. S. Novoselov, Nano Lett. **8**, 1704 (2008).

[18] Y. Hernandez, V. Nicolosi, M. Lotya, F. Blighe, Z. Sun, S. De, I. T. McGovern, B. Holland, M. Byrne, Y. Gunko, J. Boland, P. Niraj, G. Duesberg, S. Krishnamurti, R. Goodhue, J. Hutchison, V. Scardaci, A. C. Ferrari, and J. N. Coleman, Nat. Nanotechnol. **3**, 563 (2008).

[19] G. Eda, G. Fanchini, and M. Chhowalla, Nat. Nanotechnol. **3**, 270 (2008).

[20] Z. Sun, T. Hasan, F. Torrisi, D. Popa, G. Privitera, F. Wang, F. Bonaccorso, D. M. Basko, and A. C. Ferrari, arXiv:0909.0457 (unpublished); T. Gokus, R. R. Nair, A. Bonetti, M. Bohmier, A. Lombardo, N. S. Novoselov, A. K. Geim, A. C. Ferrari, and A. Hartschuh, arXiv:0909.3641 (unpublished).

[21] A. C. Ferrari, J. C. Meyer, V. Scardaci, C. Casiraghi, M. Lazzeri, F. Mauri, S. Piscanec, K. S. Novoselov, Da Jiang, S. Roth, and A. K. Geim, Phys. Rev. Lett. **97**, 187401 (2006).

[22] C. Casiraghi, A. Hartschuh, E. Lidorikis, H. Qian, H. Harutyunyan, T. Gokus, K. S. Novoselov, and A. C. Ferrari, Nano Lett. **7**, 2711 (2007).

[23] P. Blake, E. W. Hill, A. H. Castro Neto, K. S. Novoselov, D. Jiang, R. Yang, T. J. Booth, and A. K. Geim, Appl. Phys. Lett. **91**, 063124 (2007).

[24] C. Casiraghi, S. Pisana, K. S. Novoselov, A. K. Geim, and A. C. Ferrari, Appl. Phys. Lett. **91**, 233108 (2007).

[25] L. M. Malard, J. Nilsson, D. C. Elias, J. C. Brant, F. Plentz, E. S. Alves, A. H. Castro Neto, and M. A. Pimenta, Phys. Rev. B **76**, 201401(R) (2007).

[26] S. Pisana, M. Lazzeri, C. Casiraghi, K. S. Novoselov, A. K. Geim, A. C. Ferrari, and F. Mauri, Nature Mater. **6**, 198 (2007).

[27] S. Piscanec, M. Lazzeri, F. Mauri, A. C. Ferrari, and J. Robertson, Phys. Rev. Lett. **93**, 185503 (2004).

[28] L. G. Cançado, R. Beams, and L. Novotny, arXiv:0802.3709 (unpublished).

[29] C. Casiraghi, A. Hartschuh, H. Qian, S. Piscanec, C. Georgi, A. Fasoli, K. S. Novoselov, D. M. Basko, and A. C. Ferrari, Nano Lett. **9**, 1433 (2009).

[30] D. C. Elias, R. R. Nair, T. M. G. Mohiuddin, S. V. Morozov, P. Blake, M. P. Halsall, A. C. Ferrari, D. W. Boukhvalov, M. I. Katsnelson, A. K. Geim, and K. S. Novoselov, Science **323**, 610 (2009).

[31] A. C. Ferrari, Solid State Commun. **143**, 47 (2007).

[32] A. Das, S. Pisana, S. Piscanec, B. Chakraborty, S. K. Saha, U. V. Waghmare, R. Yang, H. R. Krishnamurhthy, A. K. Geim, A. C. Ferrari, and A. K. Sood, Nat. Nanotechnol. **3**, 210 (2008).

[33] A. Das, B. Chakraborty, S. Piscanec, S. Pisana, A. K. Sood, and

A. C. Ferrari, Phys. Rev. B **79**, 155417 (2009).
[34] N. Ferralis, R. Maboudian, and C. Carraro, Phys. Rev. Lett. **101**, 156801 (2008).
[35] T. M. G. Mohiuddin, A. Lombardo, R. R. Nair, A. Bonetti, G. Savini, R. Jalil, N. Bonini, D. M. Basko, C. Galiotis, N. Marzari, K. S. Novoselov, A. K. Geim, and A. C. Ferrari, Phys. Rev. B **79**, 205433 (2009).
[36] J. Yan, Y. Zhang, P. Kim, and A. Pinczuk, Phys. Rev. Lett. **98**, 166802 (2007).
[37] D. Graf, F. Molitor, K. Ensslin, C. Stampfer, A. Jungen, C. Hierold, and L. Wirtz, Nano Lett. **7**, 238 (2007).
[38] A. C. Ferrari and J. Robertson, Phys. Rev. B **61**, 14095 (2000); Phys. Rev. B **64**, 075414 (2001).
[39] *Raman spectroscopy in carbons: from nanotubes to diamond*, edited by A. C. Ferrari and J. Robertson, theme issue of Philos. Trans. R. Soc. London, Ser. A **362**, 2267 (2004).
[40] C. Thomsen and S. Reich, Phys. Rev. Lett. **85**, 5214 (2000).
[41] F. Tuinstra and J. L. Koenig, J. Chem. Phys. **53**, 1126 (1970).
[42] D. M. Basko, Phys. Rev. B **76**, 081405(R) (2007).
[43] D. M. Basko, Phys. Rev. B **78**, 125418 (2008).
[44] M. J. Martin, N. Akerman, G. Ulbricht, T. Lohmann, J. H. Smet, K. Von Klitzing, and A. Yacoby, Nat. Phys. **4**, 144 (2008).
[45] X. Wang, X. Li, L. Zhang, Y. Yoon, P. K. Weber, H. Wang, J. Guo, and H. Dai, Science **324**, 768 (2009).
[46] F. Cervantes-Sodi, G. Csanyi, S. Piscanec, and A. C. Ferrari, Phys. Rev. B **77**, 165427 (2008).
[47] M. Lazzeri and F. Mauri, Phys. Rev. Lett. **97**, 266407 (2006).
[48] M. Lazzeri, S. Piscanec, F. Mauri, A. C. Ferrari, and J. Robertson, Phys. Rev. B **73**, 155426 (2006).
[49] A. Das, A. K. Sood, A. Govindaraj, A. M. Saitta, M. Lazzeri, F. Mauri, and C. N. R. Rao, Phys. Rev. Lett. **99**, 136803 (2007).
[50] J. Yan, E. A. Henriksen, P. Kim, and A. Pinczuk, Phys. Rev. Lett. **101**, 136804 (2008).
[51] T. Ando, J. Phys. Soc. Jpn. **76**, 104711 (2007).
[52] S. Berciaud, S. Ryu, L. E. Brus, and T. F. Heinz, Nano Lett. **9**, 346 (2009); APS March Meeting Abstract, 2009, p. L26.00006.
[53] P. H. Tan, C. Y. Hu, J. Dong, W. C. Shen, and B. F. Zhang, Phys. Rev. B **64**, 214301 (2001).
[54] Y. Y. Wang, Z. H. Ni, Z. X. Shena, H. M. Wang, and Y. H. Wu, Appl. Phys. Lett. **92**, 043121 (2008); D. Yoon, H. Moon, Y.-W. Son, J. S. Choi, B. H. Park, Y. H. Cha, Y. D. Kim, and H. Cheong, Phys. Rev. B **80**, 125422 (2009); E. Lidorikis and A. C. Ferrari (unpublished).
[55] G. Landsberg and L. Mandelshtam, Naturwiss. **16**, 557 (1928); C. V. Raman and K. S. Krishnan, Nature (London) **121**, 501 (1928); **121**, 619 (1928).
[56] N. Bonini, M. Lazzeri, N. Marzari, and F. Mauri, Phys. Rev. Lett. **99**, 176802 (2007).
[57] M. Lazzeri, S. Piscanec, F. Mauri, A. C. Ferrari, and J. Robertson, Phys. Rev. Lett. **95**, 236802 (2005).
[58] R. P. Vidano, D. B. Fischbach, L. J. Willis, and T. M. Loehr, Solid State Commun. **39**, 341 (1981).
[59] I. Pócsik, M. Hundhausen, M. Koos, and L. Ley, J. Non-Cryst. Solids **227-230**, 1083 (1998).
[60] L. G. Cançado, A. Jorio, and M. A. Pimenta, Phys. Rev. B **76**, 064304 (2007).
[61] Z. Jiang, E. A. Henriksen, L. C. Tung, Y.-J. Wang, M. E. Schwartz, M. Y. Han, P. Kim, and H. L. Stormer, Phys. Rev. Lett. **98**, 197403 (2007).
[62] A. Bostwick, Solid State Commun. **143**, 63 (2007).
[63] S. Y. Zhou, D. A. Siegel, A. V. Fedorov, and A. Lanzara, Phys. Rev. B **78**, 193404 (2008).
[64] L. M. Zhang and M. M. Fogler, Phys. Rev. Lett. **100**, 116804 (2008).
[65] M. M. Fogler, D. S. Novikov, L. I. Glazman, and B. I. Shklovskii, Phys. Rev. B **77**, 075420 (2008).
[66] E. Rossi and S. Das Sarma, Phys. Rev. Lett. **101**, 166803 (2008).
[67] M. Polini, A. Tomadin, R. Asgari, and A. H. MacDonald, Phys. Rev. B **78**, 115426 (2008).
[68] J. González, F. Guinea, and M. A. H. Vozmediano, Phys. Rev. Lett. **77**, 3589 (1996) To be precise, the imaginary part of the electronic self-energy has a discontinuity on the mass shell. This discontinuity is resolved by taking into account the real part as well, which makes the electronic spectrum concave.
[69] A. A. Abrikosov and S. D. Beneslavskii, Zh. Eksp. Teor. Fiz **59**, 1280 (1970) [Sov. Phys. JETP **32**, 699 (1971)].
[70] J. González, F. Guinea, and M. A. H. Vozmediano, Mod. Phys. Lett. B **7**, 1593 (1993); Nucl. Phys. B **424**, 595 (1994); J. Low Temp. Phys. **99**, 287 (1995).
[71] E. H. Hwang, Ben Yu-Kuang Hu, and S. Das Sarma, Phys. Rev. B **76**, 115434 (2007).
[72] M. Polini, R. Asgari, G. Borghi, Y. Barlas, T. Pereg-Barnea, and A. H. MacDonald, Phys. Rev. B **77**, 081411(R) (2008).
[73] S. Latil, V. Meunier, and L. Henrard, Phys. Rev. B **76**, 201402(R) (2007).
[74] Note that substrate interference effects (Ref. 54) could mean that the measured ratios $A(2D)/A(G)$ may differ from those intrinsic to graphene by a constant factor, common for all the data points. Rescaling of the y axis in Fig. 4 by a constant factor, together with the same rescaling of the coefficient 0.26 in Eq. (6), does not affect the value of $\gamma_{\text{e-ph}}$ extracted from the fit. We note as well that the calculated rescaling of $A(2D)/A(G)$ for SiO_2 thicknesses of 0, 100, and 300 nm (i.e., those most common in experiments) is anyway negligible,[54] thus again validating our fitted $\gamma_{\text{e-ph}}$.
[75] P. R. Wallace, Phys. Rev. **71**, 622 (1947).
[76] J. Maultzsch, S. Reich, C. Thomsen, H. Requardt, and P. Ordejón, Phys. Rev. Lett. **92**, 075501 (2004).
[77] S. Piscanec, M. Lazzeri, J. Robertson, A. C. Ferrari, and F. Mauri, Phys. Rev. B **75**, 035427 (2007).
[78] M. Lazzeri, C. Attaccalite, L. Wirtz, and F. Mauri, Phys. Rev. B **78**, 081406(R) (2008).
[79] A. Grüneis, J. Serrano, A. Bosak, M. Lazzeri, S. L. Molodtsov, L. Wirtz, C. Attaccalite, M. Krisch, A. Rubio, F. Mauri, and T. Pichler, Phys. Rev. B **80**, 085423 (2009).
[80] A. Bostwick, T. Ohta, T. Seyller, K. Horn, and E. Rotenberg, Nat. Phys. **3**, 36 (2007).
[81] S. Y. Zhou, G. H. Gweon, and A. Lanzara, Ann. Phys. (N.Y.) **321**, 1730 (2006).
[82] P. E. Trevisanutto, C. Giorgetti, L. Reining, M. Ladisa, and V. Olevano, Phys. Rev. Lett. **101**, 226405 (2008).
[83] T. Ando, J. Phys. Soc. Jpn. **75**, 124701 (2006).
[84] M. Calandra and F. Mauri, Phys. Rev. B **76**, 205411 (2007).
[85] C. S. Leem, B. J. Kim, Chul Kim, S. R. Park, T. Ohta, A. Bostwick, E. Rotenberg, H.-D. Kim, M. K. Kim, H. J. Choi, and C. Kim, Phys. Rev. Lett. **100**, 016802 (2008).
[86] A. Grüneis, C. Attaccalite, A. Rubio, D. V. Vyalikh, S. L. Molodtsov, J. Fink, R. Follath, W. Eberhardt, B. Büchner, and T. Pichler, Phys. Rev. B **79**, 205106 (2009).

[87] G. Li, A. Luican, and E. Y. Andrei, Phys. Rev. Lett. **102**, 176804 (2009).

[88] D. M. Basko and I. L. Aleiner, Phys. Rev. B **77**, 041409(R) (2008).

[89] A. Grüneis, C. Attaccalite, T. Pichler, V. Zabolotnyy, H. Shiozawa, S. L. Molodtsov, D. Inosov, A. Koitzsch, M. Knupfer, J. Schiessling, R. Follath, R. Weber, P. Rudolf, L. Wirtz, and A. Rubio, Phys. Rev. Lett. **100**, 037601 (2008).